This is the accepted manuscript made available via CHORUS. The article has been published as:

Thermorefractive noise in silicon-nitride microresonators

Guanhao Huang, Erwan Lucas, Junqiu Liu, Arslan S. Raja, Grigory Lihachev, Michael L. Gorodetsky, Nils J. Engelsen, and Tobias J. Kippenberg

Phys. Rev. A **99**, 061801 — Published 24 June 2019

DOI: 10.1103/PhysRevA.99.061801

Thermo-refractive noise in silicon nitride microresonators

Guanhao Huang,[1] Erwan Lucas,[1] Junqiu Liu,[1] Arslan S. Raja,[1] Grigory Lihachev,[2,3] Michael L. Gorodetsky,[2,3] Nils J. Engelsen,[1,*] and Tobias J. Kippenberg[1,†]

[1] *Institute of Physics (IPHYS), École Polytechnique Fédérale de Lausanne, 1015 Lausanne, Switzerland*
[2] *Faculty of Physics, M.V. Lomonosov Moscow State University, Moscow 119991, Russia*
[3] *Russian Quantum Centre, 143025 Skolkovo, Russia*

(Dated: May 28, 2019)

Thermodynamic noise places a fundamental limit on the frequency stability of dielectric optical resonators. Here, we present the characterization of thermo-refractive noise in photonic-chip-based silicon nitride (Si_3N_4) microresonators and show that thermo-refractive noise is the dominant thermal noise source in the platform. We employed balanced homodyne detection to measure the thermo-refractive noise spectrum of microresonators of different diameters. The measurements are in good agreement with theoretical models and finite element method simulations. Our characterization sets quantitative bounds on the scaling and absolute magnitude of thermal noise in photonic chip-based microresonators. An improved understanding of thermo-refractive noise can prove valuable in the design considerations and performance limitations of future photonic integrated devices.

I. INTRODUCTION

Optical microresonators are used in numerous practical applications, in particular integrated, silicon-based lasers [1], narrow linewidth lasers [2] and photonic microwave oscillators [3]. The small mode volume of microresonators enables strong optical nonlinearities, harnessed in emerging technologies such as microcombs [4], and also enhances sensing capabilities used in fundamental research, e.g. cavity quantum optomechanics [5]. However, the small mode volume comes at a cost: limitations on the microresonator's frequency stability arise from thermal fluctuations such as thermo-refractive (TRN) and dimensional fluctuation thermal noise (thermoelastic and elasto-optic [6]). These fluctuations were first theoretically described in the context of laser interferometer gravitational-wave detection [7], and place limits on the frequency stability of an interferometer. Thermal fluctuations are particularly strong in small mode volume optical resonators and place fundamental limits on applications that require high frequency stability, e.g. optical sensing [8], optomechanical displacement sensing [9], dissipative Kerr soliton microcomb generation [4], electro-optical modulators [10], opto-electronic oscillators [11] and Kerr squeezing [12]. Therefore, different kinds of thermal noises have been extensively studied [7, 13–15], but theoretical analyses show inconsistencies between different platforms [16] and rely on auxiliary measurements of material parameters that are not always well-known. Experimental characterization is therefore essential to understand the limitations of a specific system.

Silicon nitride (Si_3N_4) is a space compatible [17], CMOS-compatible material [18] with a large Kerr nonlinear coefficient, an absence of two photon absorption in the telecommunication window, ultralow losses [19–21], and a wide transparency window from visible to mid-infrared. These properties have in particular been exploited for chip-scale frequency combs [4, 22–25], as well as coherent low-pulse-energy supercontinuum generation in the near- [26] and mid-infrared [27]. Recent advances [20, 28, 29] in fabrication of integrated Si_3N_4 microresonators have enabled optical quality factors $Q > 10^7$, for which TRN will impose a fundamental limit on the frequency stability, and can therefore be a limiting factor in future applications such as microwave generation [3, 30]. Although recent measurements of the carrier-envelope-offset frequency noise of microcombs [31] have already shown clear evidence that thermal noise is limiting the performance of certain applications, TRN has so far only been directly measured in simple geometries (notably silica microspheres and microtoroids [13, 32]), and has not been systematically studied in photonic integrated microresonators. Refined theoretical and modeling approaches are therefore required to analyze TRN in Si_3N_4 microresonators.

Here, we present the first characterization of TRN in Si_3N_4 microresonators, and compare finite element method (FEM) simulations with measurements of TRN using balanced homodyne detection. The results show that TRN is the dominant thermal noise source over frequencies ranging from 10 kHz to 10 MHz.

II. THERMO-REFRACTIVE NOISE

In an optical resonator, thermo-refractive noise leads to fluctuations of the resonance frequency due to fluctuations of refractive index, n, caused by thermodynamic fluctuations of temperature, δT, whose variance is:

$$\langle \delta T^2 \rangle = \frac{k_B T^2}{\rho C V} \tag{1}$$

where T is the temperature of the heat bath, k_B the Boltzmann constant, ρ the density, C the specific heat,

* nils.engelsen@epfl.ch
† tobias.kippenberg@epfl.ch

and V the volume. Using the material parameters of Si_3N_4 and the optical mode volume of a typical 1 THz free-spectral-range (FSR) microresonator, we can obtain a value of the standard deviation of the heat bath temperature as $\sqrt{\langle \delta T^2 \rangle} \sim 60\,\mu K$. Combined with the measured thermo-optic coefficient, $dn/dT = 2.45 \times 10^{-5}\,K^{-1}$, of Si_3N_4 [33], the fractional frequency fluctuation can be estimated as[13] $\sqrt{\langle \delta f^2 \rangle}/f = \frac{\sqrt{\langle \delta T^2 \rangle}}{n}\frac{dn}{dT} \sim 7 \times 10^{-10}$, and the absolute frequency fluctuation $\sqrt{\langle \delta f^2 \rangle}$ is around 150 kHz, which is up to 1% of the cavity linewidth in Si_3N_4 microresonators [29].

The thermo-refractive noise and the thermo-elastic noise, which are both consequences of thermodynamic temperature fluctuations, were previously experimentally observed in silica microspheres [13] and theoretically analyzed (but not observed) in crystalline resonators [14]. In most cases, thermo-refractive noise is the largest among the thermal noises. For chip-based Si_3N_4 microresonators, TRN is also expected to be the largest noise source, as the temperature fluctuations, which give rise to dimensional fluctuation thermal noises, are averaged over the entire resonator chip rather than the optical mode volume. However, the different modelling approaches taken in the analysis of the two previously mentioned platforms result in different predictions for the geometric dependency of TRN as well as its magnitude at low offset frequencies [16].

We now describe the two approaches taken for modelling TRN in microresonators: the first model assumes a homogeneous microresonator in an infinite heat bath, yielding the following expression for the effective temperature fluctuations: [16]:

$$S_{\delta T}(\omega) = \frac{k_B T^2}{\sqrt{\pi^3 \kappa \rho C \omega}} \sqrt{\frac{1}{2p+1}} \frac{1}{R\sqrt{d_r^2 - d_z^2}} \frac{1}{(1+(\omega\tau_d)^{3/4})^2} \tag{2}$$

where R is the ring radius of the microcavity (geometry shown in Fig. 4(a)), d_z and d_r are halfwidths of the fundamental mode with respect to the intensity, with orbital number l, azimuthal number m, meridional mode number $p = l - m$, $\tau_d = \frac{\pi^{1/3}}{4^{1/3}}\frac{\rho C}{\kappa} d_r^2$, and the definitions of the other parameters can be found in Table I. The key features are the $\omega^{-1/2}$ dependence at low frequency, the ω^{-2} dependence at high frequency, and the R^{-1} overall scaling. This model gave satisfactory agreements with experimental measurements in microspheres [13].

The second model [14] uses the thermal decomposition method which does not take into account the interaction with the environment. As a consequence, there is a low frequency cut-off due to the finite dimension of the resonator, which results in the following (single-sided) temperature noise spectral density:

$$S_{\delta T}(\omega) = \frac{k_B T^2 R^2}{12 \kappa V_{\text{eff}}} \left(1 + \left(\frac{R^2 \rho C \omega}{3^{5/3}\kappa}\right)^{3/2} + \frac{1}{6}\left(\frac{R^2 \rho C \omega}{8 l^{1/3} \kappa}\right)^2\right)^{-1} \tag{3}$$

TABLE I. **Physical properties used for both the theoretical models and FEM simulations of the thermo-refractive noise of Si_3N_4 micoresonators**

Physical properties	Values
Density (ρ)	$3.29 \times 10^3\,kg\,m^{-3}$
Refractive index (n_0)	1.996
Thermo-optic coefficient (dn/dT)	$2.45 \times 10^{-5}\,K^{-1}$
Thermal expansion coefficient $1/l(dl/dT)$	$3.30 \times 10^{-6}\,K^{-1}$
Thermal conductivity (κ)	$30\,W\,m^{-1}\,K^{-1}$
Specific heat capacity (C)	$800\,J\,kg^{-1}\,K^{-1}$

where V_{eff} is the effective mode volume. Here the expression still has a ω^2 dependence at high frequency, but features an overall scaling with R between R^{-3} and R^{-4} depending on how V_{eff} scales with radius (spherical resonator $V_{\text{eff}} \propto R^{11/6}$ or ring resonator $V_{\text{eff}} \propto R$).

The temperature fluctuations can be converted into a frequency noise spectral density through $S_{\delta f} = (f_0 \frac{1}{n_0}\frac{dn}{dT})^2 S_{\delta T}$, where f_0 is the resonance frequency. However, Eq. (2) and Eq. (3) are both idealized cases assuming homogeneous materials and either the infinite heat bath or isolated model. Clearly, these assumptions do not match the geometry of integrated Si_3N_4 resonators consisting of complex waveguide structures comprising different materials, which invalidates the assumption of homogeneity. We therefore performed an FEM simulation based on the fluctuation-dissipation theorem [15, 16], where we simulate the thermo-refractive noise of a Si_3N_4 microresonator embedded in a SiO_2 substrate, using the actual geometry. More details about the simulation can be found in the Supplemental Material [34].

We can now compare the FEM simulation results with the theoretical expressions (see Fig. 1). Because the thermal properties of Si_3N_4 depend on the material characteristics and the fabrication process, they can exhibit significant variation. We use the median values of the physical properties reported in the literature for both the theoretical predictions and the FEM simulations (see Table I). The optical mode parameters used in Eq. (2) and Eq. (3) are retrieved from FEM simulations of the Si_3N_4 microresonators. We work with fundamental modes of waveguide ring resonators ($l = m$). For the scaling with ring radius, the simulation curves match the infinite heat bath theory Eq. (2) well, while the deviation from the thermal decomposition method becomes larger as the radius increases. It indicates that, according to FEM simulations, Si_3N_4 microresonators experience thermo-refractive noise more similar to microspheres at high frequency, while at low frequency, the noise is reduced due to the cladding region (SiO_2) and the chip geometry. The measurement results, the simulation curves and the infinite heat bath curves are compared in Fig. 4.

Due to the R^{-1} scaling and the strong light confinement the Si_3N_4 waveguide offers, the computed spectral density of thermo-refractive frequency noise for resonators with FSR ranging from 20 GHz and 1 THz is sufficiently high to be probed without an extremely pure and stable laser. In crystalline microresonators, the

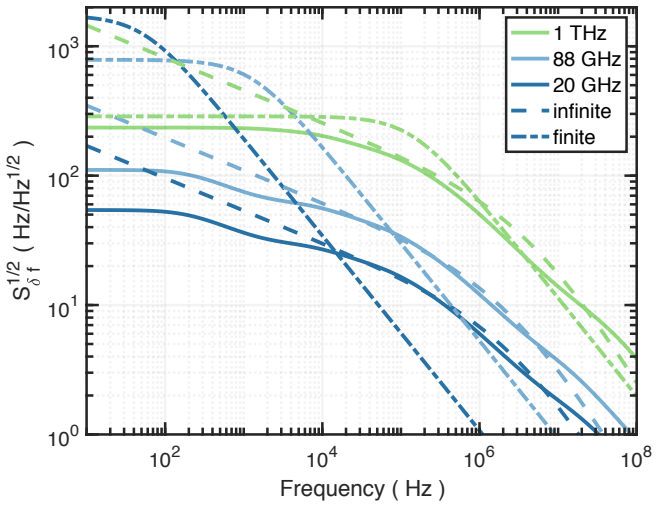

FIG. 1. **Comparison of FEM simulation results of thermo-refractive noise with the theoretical predictions (infinite heat bath and thermal decomposition).** The graphs show the cavity frequency noise spectral density of a Si_3N_4 microresonator with a free spectral range (FSR) of 1 THz, 99 GHz and 20 GHz. At high frequency, the simulation curves match better with the infinite heat bath assumption. At low frequency, the simulation curves experience a cut-off because of the finite size of the modelled chip, which behaves more similar to the thermal decomposition method.

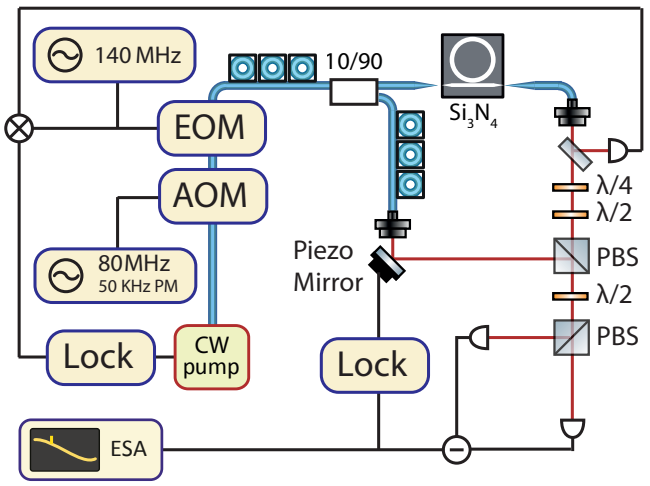

FIG. 2. **Balanced homodyne setup for measuring thermo-refractive noise of the Si_3N_4 microresonator.** The electro-optic modulator (EOM) phase-modulates the light at 140 MHz to generate the PDH error signal for locking the laser to the cavity mode. The AOM is modulated with an RF tone with a central frequency of 80 MHz. The RF tone is then phase modulated at 50 kHz with a 1.14 rad modulation depth, which provides an absolute calibration peak for the noise measurements. A piezo mirror is used in the local oscillator path to lock the homodyne at the phase quadrature. The measurement bandwidth is limited by the detector bandwidth of 80 MHz.

much larger mode volume and smaller thermo-optic coefficient (dn/dT) make it much more challenging to measure TRN [35], and correspondingly it is typically not a practical limit.

III. MEASUREMENT SCHEME AND RESULTS

The measurement scheme in this study (illustrated in Fig. 2) employs a balanced homodyne setup to measure the phase fluctuations of the transmitted light caused by the cavity frequency noise. The cavity frequency noise is calibrated using a calibration tone. The laser (external cavity diode laser at 1550 nm with a linewidth of $\sim$ 30 kHz) is locked to the cavity resonance via the Pound-Drever-Hall (PDH) locking method [36] with a feedback bandwidth of a few kilohertz. We characterize the phase noise of the laser (see Supplemental Material [34]) and subtract it from the measurement traces for the 100 GHz and 200 GHz-FSR data shown in Fig. 4. The power level is sufficiently low to avoid any unwanted thermal effects.

In order to provide an absolute calibration of our measurement, we use a calibration tone generated by phase modulating the RF tone applied to the acousto-optic modulator (AOM). A modulation depth of 1.14 rad is calibrated by sideband fitting using heterodyne detection. The calibration tone induces an extra phase fluctuation transduced by the cavity, and results in a narrow peak in the frequency noise spectrum. Because the frequency modulation depth is known for the calibration peak, we can use it to calibrate the absolute magnitude of the corresponding homodyne signal. The modulation frequency and the modulation depth are chosen at 50 kHz and 1.14 rad to be outside the PDH locking bandwidth and to keep the frequency modulation depth smaller than the cavity linewidth.

The characterized samples are integrated Si_3N_4 microresonators with radius $R \sim 23 - 1200\,\mu$m, and FSR ranging from 1 THz to 20 GHz. The Q-factors of these microresonators fabricated by the photonic Damascene reflow process [28, 29] are typically $Q > 10^7$. The measured noise spectrum is thus filtered by the cavity resonance at high offset frequencies. The resonance linewidth of each microresonator and the response function of the bias tee before the spectrum analyzer are measured and compensated for through data post-processing.

We first verified the power-independent nature of thermo-refractive noise (as expected from Eqs.1-3) by performing an input power sweep (shown in Fig. 3). The frequency noise level remains the same when varying the laser power of the probe signal by more than two orders of magnitude (from 1 µW to 120 µW), showing that photothermal noise is not making a significant contribution. We next investigated the dependence on optical mode volume. Fig. 4 (c) presents the measurement results for four different cavity radii, together with the corresponding theoretical curves and FEM simulation curves. The

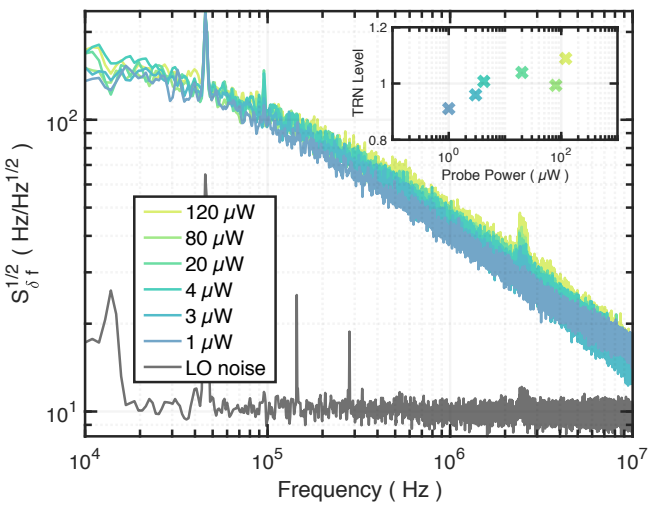

FIG. 3. **Calibrated thermo-refractive frequency noise spectra measured using different probing power.** A Si_3N_4 microresonator with free spectral range of 1 THz was probed with 1 µW to 120 µW of optical power. The the bottom line shows the shot noise level with 1 µW of input optical power. The normalized units utilized in the inset figure are obtained by integrating over 200 kHz to 2 MHz and dividing by the average of the integrated values. It indicates that the probe is weak enough to avoid other laser-induced thermal effects (e.g. photothermal noise), and importantly reveals the power-independence expected for thermo-refractive noise.

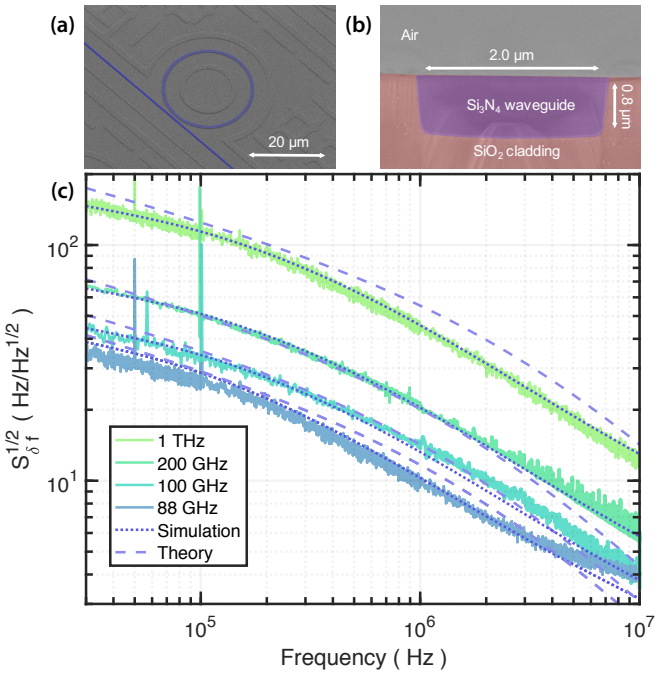

FIG. 4. **Verification of the size dependence of thermo-refractive noise in integrated Si_3N_4 microresonators.** **(a)** SEM image of a 1 THz-FSR Si_3N_4 microresonator ring (dark blue). **(b)** SEM image of the cross-section of the waveguide. The cross-section image is color shaded to help identify different regions. **(c)** Thermo-refractive noise measured in integrated Si_3N_4 microresonators with free spectral ranges of 1 THz, 200 GHz, 100 GHz and 88 GHz. The 88 GHz-FSR sample has a bigger width (2.0 µm) compared to other samples (1.5 µm) and there is some run to run variation in sidewall angles. A 30-point moving average was applied to the data. The dotted lines show the FEM simulation results and the dashed lines show the theoretical predictions from Eq. (2). Data below 10 kHz were truncated due to the excess locking noises, and also data above 10 MHz due to the detector's nonlinear response. Additional data can be found in the Supplemental Material [34].

observable background noise sources arise from local oscillator shot noise, several technical spikes, and the calibration peak at 50 kHz. The calibration peaks in the off-resonance noise spectrum and the LO shot noise spectrum (see Supplemental Material [34]) are the result of residual amplitude modulation from the AOM. However, by utilizing phase modulation of the AOM RF tone, a signal-to-noise ratio of 20 dB can be obtained for the calibration peak.

Good agreement of the measured spectra with the simulation curves for both frequency dependence ($\propto \omega^{-1/2}$) and radius dependence ($\propto R^{-1}$) is clearly observed, which also confirms the validity of Eq. (2) as a theoretical prediction of TRN (at frequency above 10 kHz) in the Si_3N_4 microresonator platform. By assuming that the spectrum matches the FEM simulation in the low frequency range, the total frequency fluctuations due to TRN could be retrieved through integration over the high frequency experimental data and the low frequency FEM curves (the latter contributes less than 1% of the total frequency variance), e.g. the 1 THz microresonator has a resonance frequency instability of around 240 kHz, which agrees well with our previous estimation of 150 kHz. The agreement further indicates that the heat exchange with the surrounding environment is largely responsible for the generation of thermo-refractive noise in this system. However, in the low frequency range, the approximation of a homogeneous medium in Eq. (2) will break down due to heat exchange with the media outside the waveguide, as is indicated by the multiple saturation steps of the FEM simulation curves at low frequency shown in Fig. 1. Though the heat exchange with the outer layer makes it difficult to derive a simple expression for the thermo-refractive noise in Si_3N_4 microresonators, it offers a possibility to bypass the thermal limit [37]. The design of such a thermal-noise-reduced photonic microresonator will be more important when more applications truly reach the thermal limit of their performance, e.g. to realize integrated ultra narrow linewidth lasers.

IV. CONCLUSION

We present the first characterization of thermo-refractive noise in the integrated Si_3N_4 microresonator platform. The presence of thermo-refractive noise in

photonic integrated resonators could limit the performance for many applications. Therefore, we measured the thermo-refractive noises of Si_3N_4 microresonators with a wide range of FSR. The measurement results are in good agreement with both the FEM simulation and the theoretical prediction for both frequency dependence ($\propto \omega^{-1/2}$) and radius dependence ($\propto R^{-1}$). The characterization of thermo-refractive noise in Si_3N_4 microresonator systems can serve as a standard for comparison of the noise features observed in associated applications such as microwave generation. Finally, these results might provide new insights for the silicon photonics community, enabling a better understanding of the formation of thermo-refractive noise as well as a path towards systems which bypass thermal noise limitations.

DATA AVAILABILITY STATEMENT

Data and data analysis code will be made available through `Zenodo` upon publication. All other data needed to evaluate the conclusions in the paper are present in the paper or the supplemental materials.

FUNDING INFORMATION

This publication was supported by Contract HR0011-15-C-0055 from the Defense Advanced Research Projects Agency (DARPA), Microsystems Technology Office (MTO), and Contract HR0011181003 from DARPA, Defense Sciences Office (DSO), by the Swiss National Science Foundation under grant agreement No.163864, and the Russian Foundation for Basic Research project 17-02-00522.

ACKNOWLEDGMENTS

All samples were fabricated at the Center for MicroNanoTechnology (CMi) at EPFL. We acknowledge Rui Ning Wang for the assistance in sample fabrication.

[1] D. Liang and J. E. Bowers, Nature Photonics **4**, 511 (2010).
[2] S. Gundavarapu, G. M. Brodnik, M. Puckett, T. Huffman, D. Bose, R. Behunin, J. Wu, T. Qiu, C. Pinho, N. Chauhan, *et al.*, Nature Photonics **13**, 60 (2019).
[3] W. Liang, D. Eliyahu, V. S. Ilchenko, A. A. Savchenkov, A. B. Matsko, D. Seidel, and L. Maleki, Nature communications **6**, 7957 (2015).
[4] T. J. Kippenberg, A. L. Gaeta, M. Lipson, and M. L. Gorodetsky, Science **361**, eaan8083 (2018).
[5] M. Aspelmeyer, T. J. Kippenberg, and F. Marquardt, Reviews of Modern Physics **86**, 1391 (2014).
[6] A. Chijioke, Q.-F. Chen, A. Y. Nevsky, and S. Schiller, Physical Review A **85**, 053814 (2012).
[7] V. Braginsky, M. Gorodetsky, and S. Vyatchanin, Physics Letters A **271**, 303 (2000).
[8] M. R. Foreman, J. D. Swaim, and F. Vollmer, Adv. Opt. Photon. **7**, 168 (2015).
[9] G. Anetsberger, E. Gavartin, O. Arcizet, Q. P. Unterreithmeier, E. M. Weig, M. L. Gorodetsky, J. P. Kotthaus, and T. J. Kippenberg, Physical Review A **82**, 061804(R) (2010).
[10] N. G. Pavlov, N. M. Kondratyev, and M. L. Gorodetsky, Appl. Opt. **54**, 10460 (2015).
[11] L. Maleki, in *2012 European Frequency and Time Forum* (IEEE, 2012) pp. 497–500.
[12] U. B. Hoff, B. M. Nielsen, and U. L. Andersen, Optics Express **23**, 12013 (2015).
[13] M. L. Gorodetsky and I. S. Grudinin, J. Opt. Soc. Am. B **21**, 697 (2004).
[14] A. B. Matsko, A. A. Savchenkov, N. Yu, and L. Maleki, J. Opt. Soc. Am. B **24**, 1324 (2007).
[15] W. Weng, P. S. Light, and A. N. Luiten, Optics Letters **43**, 1415 (2018).
[16] N. Kondratiev and M. Gorodetsky, Physics Letters A **382**, 2265 (2018).
[17] V. Brasch, Q.-F. Chen, S. Schiller, and T. J. Kippenberg, Optics Express **22**, 30786 (2014).
[18] D. J. Moss, R. Morandotti, A. L. Gaeta, and M. Lipson, Nature Photonics **7**, 597 (2013).
[19] M. H. Pfeiffer, A. Kordts, V. Brasch, M. Zervas, M. Geiselmann, J. D. Jost, and T. J. Kippenberg, Optica **3**, 20 (2016).
[20] X. Ji, F. A. Barbosa, S. P. Roberts, A. Dutt, J. Cardenas, Y. Okawachi, A. Bryant, A. L. Gaeta, and M. Lipson, Optica **4**, 619 (2017).
[21] J. F. Bauters, M. J. Heck, D. D. John, J. S. Barton, C. M. Bruinink, A. Leinse, R. G. Heideman, D. J. Blumenthal, and J. E. Bowers, Optics Express **19**, 24090 (2011).
[22] T. J. Kippenberg, R. Holzwarth, and S. A. Diddams, Science **332**, 555 (2011).
[23] M. H. Pfeiffer, C. Herkommer, J. Liu, H. Guo, M. Karpov, E. Lucas, M. Zervas, and T. J. Kippenberg, Optica **4**, 684 (2017).
[24] Q. Li, T. C. Briles, D. A. Westly, T. E. Drake, J. R. Stone, B. R. Ilic, S. A. Diddams, S. B. Papp, and K. Srinivasan, Optica **4**, 193 (2017).
[25] T. C. Briles, J. R. Stone, T. E. Drake, D. T. Spencer, C. Fredrick, Q. Li, D. Westly, B. Ilic, K. Srinivasan, S. A. Diddams, *et al.*, Optics Letters **43**, 2933 (2018).
[26] A. R. Johnson, A. S. Mayer, A. Klenner, K. Luke, E. S. Lamb, M. R. Lamont, C. Joshi, Y. Okawachi, F. W. Wise, M. Lipson, and A. Gaeta, Optics Letters **40**, 5117 (2015).
[27] H. Guo, C. Herkommer, A. Billat, D. Grassani, C. Zhang, M. H. Pfeiffer, W. Weng, C.-S. Brès, and T. J. Kippenberg, Nature Photonics **12**, 330 (2018).
[28] M. H. P. Pfeiffer, C. Herkommer, J. Liu, T. Morais, M. Zervas, M. Geiselmann, and T. J. Kippenberg, IEEE Journal of Selected Topics in Quantum Electronics **24**, 1 (2018).
[29] J. Liu, A. S. Raja, M. Karpov, B. Ghadiani, M. H. P. Pfeiffer, B. Du, N. J. Engelsen, H. Guo, M. Zervas, and

T. J. Kippenberg, Optica **5**, 1347 (2018).
[30] J. Liu, E. Lucas, A. S. Raja, J. He, J. Riemensberger, R. N. Wang, M. Karpov, H. Guo, R. Bouchand, and T. J. Kippenberg, arXiv preprint arXiv:1901.10372 (2019).
[31] T. E. Drake, J. R. Stone, T. C. Briles, D. T. Spencer, and S. B. Papp, in *Frontiers in Optics* (Optical Society of America, 2018) pp. JTu2A–62.
[32] O. Arcizet, R. Rivière, A. Schliesser, G. Anetsberger, and T. J. Kippenberg, Phys. Rev. A **80**, 021803(R) (2009).
[33] A. Arbabi and L. L. Goddard, Optics Letters **38**, 3878 (2013).
[34] See Supplemental Material at [URL] for more details about the simulations and additional measurements.
[35] J. Lim, A. A. Savchenkov, E. Dale, W. Liang, D. Eliyahu, V. Ilchenko, A. B. Matsko, L. Maleki, and C. W. Wong, Nature Communications **8**, 8 (2017).
[36] R. Drever, J. L. Hall, F. Kowalski, J. Hough, G. Ford, A. Munley, and H. Ward, Applied Physics B **31**, 97 (1983).
[37] H. J. Kimble, B. L. Lev, and J. Ye, Phys. Rev. Lett. **101**, 260602 (2008).